High-Pressure Investigation of 2,4,6-Trinitro-3-bromoanisole (TNBA): Structural Determination and Piezochromism

Christian M. Childs,* Brad A. Steele, Paulius Grivickas, Dongzhou Zhang, Jonathan Crowhurst, I-Feng W. Kuo, Sorin Bastea, and Samantha M. Clarke

ACCESS | 📊 Metrics & More | 📑 Article Recommendations | 🆂🅸 Supporting Information

ABSTRACT: Understanding phase transitions in energetic materials is crucial for developing predictive models of detonation. 2,4,6-Trinitro-3-bromoanisole (TNBA), an energetic material, was studied in its single-crystal form up to pressures of 45 GPa in a diamond anvil cell. The material was characterized by using X-ray, Raman, and optical transmission measurements. From single-crystal X-ray diffraction, the ambient structure of TNBA was determined which crystallizes in the $P2_1/c$ space group having four molecular units per unit cell. The X-ray data up to 9.2 GPa were fitted to a third-order Birch−Murnaghan equation of state by using the parameters $K_0 =$ 13.2(2.4) GPa and $K_p = 5.1(1.4)$. Between 6.8 and 7.3 GPa, a phase transition was inferred in TNBA from concurrent fading of X-ray diffraction, disappearance of Raman peaks, increase in sample fluorescence, and discontinuous color change. The new phase was consistent with an amorphous state of at least partially intact molecules judging from the presence of higher-order Raman modes and irreversibility of the Raman spectra upon release. Piezochromism was observed with the translucent yellow TNBA gradually darkening and becoming opaque black at ~25 GPa. This correlated to the absorption edge gradually shifting to the red in the visible spectrum. Signs of two possible additional structural transitions were detected in the 32.4−41.0 GPa range as suggested by a jump in the absorption edge, the irreversible changes in the absorption spectrum upon release to ambient pressure, and by the lack of Raman modes in recovered samples. The crystal and electronic structures of TNBA were also investigated up to 10 GPa by using DFT calculations and crystal structure prediction (CSP) simulations. In agreement with the experimentally observed transition at 7 GPa, the simulations at 10 GPa found a bevy of polymorphs lower in enthalpy and higher in density than $P2_1/c$. The lowest calculated enthalpy structure was determined to be $P2_12_12_1$, being in a different space group than the ambient experimental result.
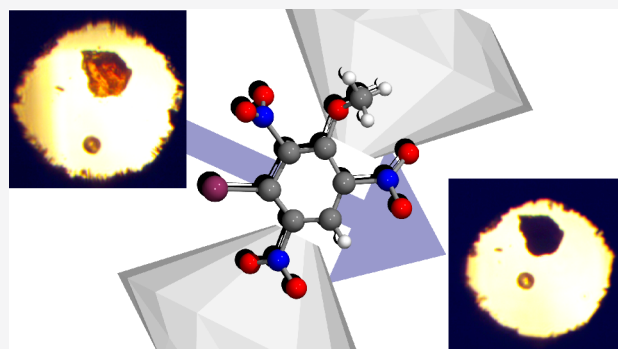
INTRODUCTION

There is continuing interest in the development of new energetic materials (EM) which are safer, more reliable, and manufactured by more environmentally friendly processes. Historically, 2,4,6-trinitrotoluene (TNT) is one of the standard EMs used to compare the yield of explosive events, and it is still manufactured in high volumes for different applications. Recently, 2,4,6-trinitro-3-bromoanisole (TNBA) was synthesized and has been shown to have molecular structure very similar to TNT, except for the methyl group which is replaced by a methoxy group and for one of the hydrogen atoms which is replaced by a bromine atom as shown in Figure 1. Therefore, it was not surprising that impact and spark sensitivity of this novel EM were similar to TNT,[1,2] and this material retains the same benefit of melt casting capability (meting temperature of 95−100 °C[1,2] as compared to 80 °C in TNT and decomposition temperature of 260 °C[1,2] as compared to 264 °C in TNT). However, it was found that TNBA has an advantage in its simple synthesis route: one-step nitration

followed by precipitation of a crystalline solid in high yields (96.5−100%)[1,2] as compared to the manufacturing process of TNT which produces a toxic red wastewater.[3]

Many different properties influence the sensitivity of energetic materials[4] such as compressibility, lattice free volume,[5,6] and the polymorphic form of the material.[7,8] While the molecular structure of energetic materials is responsible for the chemical mechanism of the initiation, the crystal structure or polymorph of the material affects the physicochemical responses and performance characteristics.[4,5,7−9] Thus, the knowledge of an EM's crystal structure in its ambient form as well as its phases occurring at higher
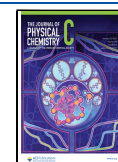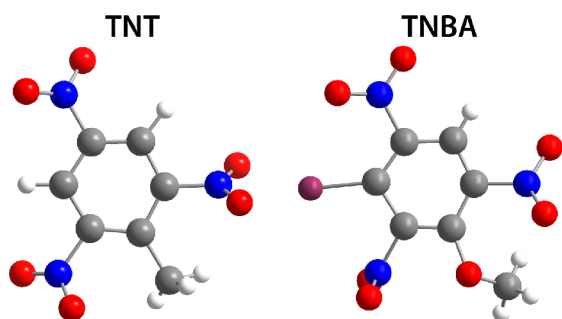
Figure 1. Molecular structure of TNT and TNBA. Gray = carbon, blue = nitrogen, red = oxygen, white = hydrogen, and magenta = bromine. TNBA is similar to TNT in that it is a aromatic with three nitro groups. Replacing the methyl group in TNT with a methoxy group and a hydrogen with a bromine yields TNBA. Additionally, when TNBA is in its crystalline ambient form, one of the nitro groups is oriented perpendicular to the plane of the phenyl ring.

pressures is crucial in understanding its reacted equation of state (EOS) and predictive modeling in detonation simulations.

To the authors' knowledge, the crystal structure of TNBA has not been reported yet, and no high-pressure studies exist in the open literature. In this work we perform the first structural determination of TNBA using single-crystal X-ray diffraction (SCXRD) and investigate possible phase changes of this EM at isothermal high-pressure conditions using Raman spectroscopy and visible absorption. In addition, we conduct energy minimization DFT calculations and crystal structure prediction (CSP) simulations to guide and support experimental findings.

■ METHODS

Experimental Section. Crystalline TNBA was used as received from Picatinny Arsenal. The sample came as yellowish small crystallites which were either loaded as a single crystal or conglomerated as a powder into diamond anvil cells. Table 1

Table 1. Table of Loadings Used in This Work

loading	cell type	PTM	measurements	press. range (GPa)
A	One20	Ne	SCXRD	0.8−9.2
B	symmetric	none	PXRD	ambient
C	symmetric	Ne	absorption, Raman	0.5−45
D	symmetric	Ar	absorption, Raman	1.2−8
E	BX-90	NaCl	Raman	0−8
F[a]	symmetric	He	PXRD	1.1−19.4

[a]Loading F is reported in the Supporting Information (Figure S1).

shows a total of six diamond anvil cell loadings that are reported in this work. The loadings A and B were used for the single-crystal X-ray diffraction and powder diffraction experiments, respectively. Loadings C, D, and E were in three different pressure transmitting mediums (neon, argon, and NaCl) and were used for simultaneous Raman spectroscopy and visible absorption measurements. Loading F was powder TNBA in helium, and it was found that helium permeated the molecular crystal (see the Supporting Information).

Loadings A, B, and F had X-ray diffraction taken at the same beamline. In the course of our high-pressure X-ray diffraction (XRD) experiments, we observed the appearance of irreversible color centers and subsequent amorphization of the material when it was investigated under high X-ray flux at an

APS undulator station using energies above 33 keV. Thus, the sample was then investigated at lower energies and fluences at beamline 13-BM-C, GeoSoilEnviroCARS, Advanced Photon Source, Argonne National Laboratory. The X-ray energy was set to 28.6 keV (0.434 Å), and the focused X-ray spot was 12 × 18 μm^2. Data were collected on a Pilatus 1M detector. Calibration of sample−detector distance, tilt, and geometric distortions were obtained from a NIST LaB$_6$ diffraction standard. After increasing pressure, data collection was started with a delay of at least 20 min to minimize the effect of gasket creep during data acquisition. Runs using a helium pressure transmitting medium (loading F) yielded unit cells of greater volume than when in neon above 5 GPa, indicating helium permeation into the molecular crystal (see the Supporting Information). Thus, all reported experiments were done in a neon, argon, or NaCl environment.

For the single-crystal X-ray diffraction (SCXRD) experiment (loading A), a gasketed Almax One20 diamond anvil cell (DAC) was loaded in air with one single crystal and one ruby and then high-pressure gas loaded with neon as a hydrostatic pressure transmitting medium (PTM).[10] Rhenium gaskets, preindented to 40−45 μm thick by using 300−400 μm culets, were used to radially confine the samples. Initial sample chamber diameters were approximately 175−200 μm, and the sample dimensions were approximately 20 × 50 μm^2. Pressures were measured by ruby fluorometry using the revised scale of Shen et al.[11] All error bars on pressure readings represent the expected nonhydrostatic stress pressure deviation in neon from Klotz et al.[10] and the pressure drift from before and after the measurement. Data were collected over a 100°−110° angular range around ϕ = 0.00° in 1.00° steps with an acquisition time of 20−50 s per step. Reciprocal space sampling is limited because of the aperture of the diamond anvil cell and because of the X-ray focusing optics which prevented collecting redundant reflections around ϕ = 180°. The SCXRD data were analyzed by using APEX3 and Olex2[12] software. Analytical absorption corrections on the raw diffraction peaks were performed with the program SADABS.[13]

Loading B had powder X-ray diffraction (PXRD) taken at ambient pressure and temperature in a symmetric type diamond anvil cell at the same beamline as the SCXRD. Integration of the powder diffraction images to yield 2θ versus scattering intensity patterns was performed by using the DIOPTAS program.[14] Analysis of the X-ray diffraction patterns was performed by using GSAS II.[15] Crystal structure prediction was performed by using Vesta[16] and Diamond software.

DAC loadings C, D, and E were used for Raman spectroscopy and visible absorption measurements. Loadings C and D used symmetric type diamond anvil cells with 300 μm culets. Single crystals of TNBA were loaded in a neon PTM (C) and an argon PTM (D) into the symmetric cells. Loading E was TNBA powder in a BX90 DAC with 400 μm culets in an NaCl PTM. While using 514.5 nm as a laser source, we observed fluorescence of the sample above a few milliwatts of laser power at ambient pressure. Thus, around 1−3 mW of 632.8 nm was used as a laser source on loadings C and D and ~0.2 mW on the loading E. The D loading in argon was compressed to 7.8(1) GPa and back to ambient pressure to test for irreversibility of the observed transition at 7 GPa. The C loading in neon was compressed to 44.8(2) GPa and back to ambient pressure. The E loading in NaCl was compressed to 8(1) GPa.

All of the absorption and Raman measurements were taken with a custom-built optical system. A 300 grooves/mm grating was used for the absorption measurements, and an 1800 grooves/mm grating was used for the Raman measurements. A stable tungsten light source (Thorlabs SLS201L) was used for transmission lighting of the sample chamber. The spectral detection range of the system is approximately 450−900 nm. A spatial filter was used to collect light from a circular region 20 μm in diameter in the sample chamber. The sample size was roughly 60−100 μm wide in all loadings. For each pressure point, a reference spectrum was taken through the PTM, and a spectrum was taken through the sample. During the course of the experiment, no visible change to the sample surface or geometry was observed; thus, no significant changes to the sample's scattering coefficient are expected.

Simulations. TNBA was investigated by using density functional theory (DFT)[17,18] as implemented in the Vienna Ab initio Simulation Package[19] (VASP) by using projector-augmented wave (PAW) pseudopotentials.[20,21] The Perdew−Burke−Ernzerhof (PBE)[22] generalized gradient approximation functional was used with the Grimme D2 empirical correction (PBE+D2) to account for van der Waals forces that are poorly described by DFT.[23−25] PBE with van der Waals empirical correction has previously been shown to yield fairly good results compared to experiment for the EOS and vibrational properties of other CHNO molecular crystals.[26−28] TATB is somewhat similar to TNBA because they both contain trinitrobenzene rings but differ at the other three sites of the benzene ring. The crystal structure is also layered like TATB. In TATB, the hydrogen-bonding interactions between amino and nitro groups were found to be too weak by using PBE+D2 but were more accurate by using PBE0+D2.[28] However, PBE0+D2 seemed to describe the strength of van der Waals interactions between the planes too strongly.[28] Results for TNBA may be similar.

The isothermal (at $T = 0$ K), unreacted equation of state (EOS) of the ambient phase of TNBA was found by optimizing the lattice parameters, atomic configurations, and hydrostatic pressure as a function of volumetric compression ratio V/V_0. The equilibrium volume V_0 was calculated at ambient pressure, and the volume was reduced sequentially in increments of $0.02V_0$. The wave function was calculated with a 900 eV plane-wave energy cutoff and k-point density of 0.05 Å^{-1} for the smallest volume studied, a $3 \times 3 \times 3$ k-point grid. The self-consistent field accuracy threshold was set to 1×10^{-8} eV, and optimizations of the ionic degrees of freedom were performed with a force-based accuracy threshold of 1×10^{-2} eV/Å. The zero-point energy (ZPE) and entropic contribution to the free energy were not included but have been investigated for other energetic materials.[26−28]

A molecular crystal structure search of high-pressure polymorphs was performed at 10 GPa, and a validation search was performed at 0 GPa by using the first-principles evolutionary crystal structure prediction method USPEX.[29−31] The molecular search algorithm and variation operators are described in more detail in ref 32. The search seeds whole molecules of TNBA, and they are allowed to be flexible. There are no explicit constraints on the space group or lattice parameters. The initial volume estimate is equal to the unit cell volume of the ambient phase at 0 and 10 GPa. The minimal distance between centers of molecules was set to 1.6 Å, and the atomic distance constraints were set to 0.6−0.7 times the minimum distance between atoms for the ambient

phase. The enthalpies were calculated with a similar DFT approach for the USPEX search as for the EOS calculation described above, with exceptions noted below. A plane-wave energy cutoff of 520 eV and k-point density of 0.12 Å^{-1} were used during the search for computational efficiency. 0.12 Å^{-1} was found to be sufficient because the unit cell volume changes by only 0.78% and 0.21% calculated with a k-point spacing of 0.05 Å^{-1} at 0 and 10 GPa, respectively. The search was performed with 4 formula units in the unit cell. At 0 GPa, the search was performed for 13 generations and produced a total of 900 structures, and at 10 GPa the search was performed for 10 generations and produced 621 structures. The lowest energy molecular polymorph did not change after the first generation, so the speed at which low-energy polymorphs were produced relative to the computational cost was low; therefore, the search was stopped. The search was not successful at finding the ambient phase crystal structure but was successful at finding energetically competitive structures within just 1 kcal/mol at 0 GPa.

■ RESULTS

X-ray Diffraction. *Ambient Structure.* While the energetic[1,2,33,34] and toxicologic[35,36] properties of TNBA have been previously reported, the crystal structure and high-pressure properties have remained unknown. To determine the crystal structure of TNBA and understand the response of the structure to pressure, we performed powder X-ray diffraction (PXRD) and single-crystal X-ray diffraction (SCXRD) at GSECARS, APS. Because of time constraints at the beamline, loading A was gas loaded before beamtime, and the structure was solved at the gas loaded pressure of 0.8(2) GPa. We believe this is still the same structure as the ambient structure since powder X-ray diffraction from ambient to 1 GPa (loading F) shows no evidence of any phase transition (Figure S1).

The full crystal structure at 0.8(2) GPa in a neon PTM (loading A) was solved by using APEX3 for data integration and reduction and Olex2[12] for structure solution and refinement. Refining the structure while fixing only hydrogen positions yielded a fit of an R_1 = 7.1%. The molecule crystallizes in the monoclinic space group $P2_1/c$ with four molecular units per unit cell. It is a layered structure where every third layer overlays each other (ABC motif) as seen in Figure 2. Using the structure solved through SCXRD, we have indexed the ambient structure's parameters using both PXRD at ambient pressure and SCXRD from 0.8 to 9.2 GPa. The unit cell parameters at ambient from PXRD (loading B) are a = 10.791(15) Å, b = 9.179 8(38) Å, c = 12.012(18) Å, θ = 115.302(34)°, and V = 1075.78(53) Å^3. Table S1 shows the fractional coordinates and lattice information about the atoms found from our solution (see the Supporting Information for a crystallographic information file).

To help establish a baseline for the comparison between experiment and theory, the lattice parameters at 0 GPa were compared, displayed in Table 2. The calculated lattice parameters are at 0 K, while experiment is at room temperature. The overall accuracy of 3−5% of experiment is within a reasonable error so qualitative conclusions can be made as a function of pressure. The results are comparable to a similar molecule, TATB, where thermal expansion from 0 K to room temperature and zero-point energy effects produced an anisotropic thermal expansion of about 0.75% in the planar direction of the molecules and 4% perpendicular to the planes at the PBE+D2 level.[28]
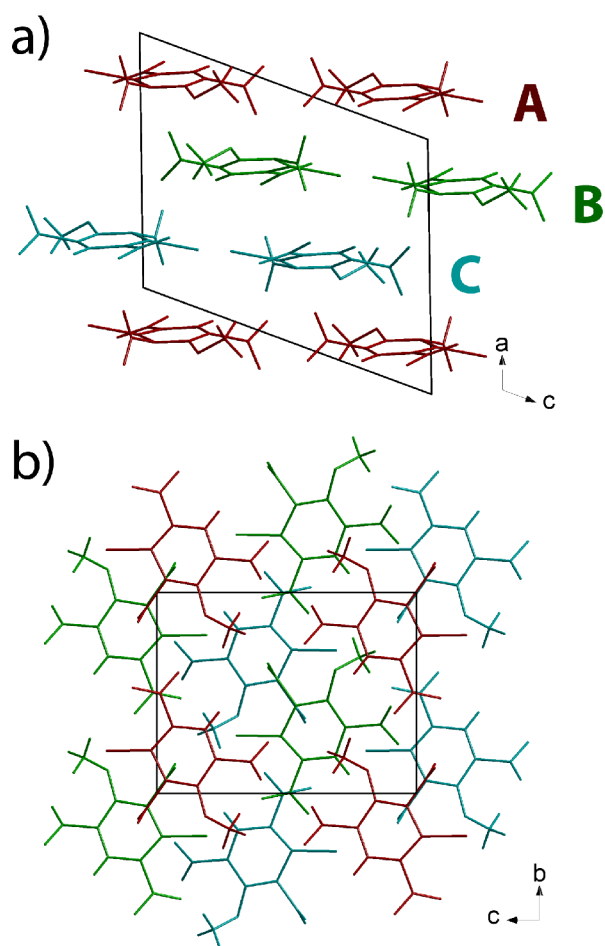
Figure 2. Structure of TNBA is a layered structure with an ABC packing arrangement. (a) Monoclinic unit cell of TNBA viewed along the *b*-axis. (b) Monoclinic unit cell of TNBA viewed along the *a*-axis, showing only three layers.

The errors in the calculated lattice parameters are correlated to different types of interactions in the crystal. For example, the *a* lattice parameter is approximately perpendicular to the planes of the molecules and may be the most dependent on van der Waals interactions. The predicted *a* lattice parameter of TNBA is 3.24% less than the experimental value. This error is primarily due to thermal expansion from 0 K to room temperature and partially because DFT describes van der Waals interactions poorly. The *b* lattice parameter is

approximately in the plane of the molecules and includes interactions between the methyl and nitro group. The strength of the hydrogen bond may be underpredicted by using PBE +D2.[28] The predicted *b* lattice parameter is only 0.29% smaller than experiment, which means at room temperature the magnitude of the difference will be slightly larger. The *c* lattice parameter is partially in the plane and out of the plane and may be dependent on interactions between bromine and the nitro group. The error in the predicted *c* lattice parameter is the largest, 3.21% larger than experiment, which would be larger in magnitude at room temperature. This indicates there may be an error associated with modeling the interactions with bromine using a standard GGA DFT functional.[37−39] Structural studies may be performed in the future with different functionals to evaluate the accuracy of DFT.

Equation of State. Under pressure in a neon environment (loading A), the sample maintains its crystallinity up to 9.2(3) GPa as evidenced by presence of reflections in SCXRD. As pressure is increased, the higher angle reflections decrease in intensity with increasing pressure, which is a characteristic signature of increasing mosaicity of the crystal (Figure S2).[40]

We see the low order modes of the Raman spectra broaden (in loading C) roughly in the same pressure range that we see the XRD mosaicity (∼2−7 GPa).

Given that we see mosaicity well before the neon crystallizes, any deviatoric stress that could be causing this mosaicity is not coming from the PTM. Above 9.2 GPa we see no reflections below 2.5 Å, and the crystallinity is too poor to determine the unit cell parameters. Because of loss of diffraction and Raman above 9 GPa, this study is unable to definitively identify a high-pressure phase or if the system is amorphous. Any amorphous X-ray diffraction that may be present is lost in the background noise in our data as X-ray diffraction of an amorphous material is weak compared to single-crystal peak Bragg diffraction. Although no direct measurement of amorphization was obtained, the loss of X-ray diffraction and Raman indicate either amorphization or nanocrystal domains.

Table 2 shows the measured lattice parameters of TNBA in Ne PTM up to 9.2(3) GPa. Figure 3 shows the third-order Birch−Murnaghan equation of state fit to the loading in neon up to 9.2 GPa. There is a slight deviation from the Birch−Murnaghan fit at 7 and 9 GPa; however, they are both within error of the fit.

The deviation in volume in the XRD from 7 to 9 GPa could be due to phase coexistence in the sample, which would coincide with the Raman and absorption transition of 7 GPa.

Table 2. Lattice Parameters of Monoclinic TNBA[a]

source	*P* (GPa)	*a* (Å)	*b* (Å)	*c* (Å)	*θ* (deg)	*V* (Å³)
calc'd(0 K)	0	10.441(−3.2%)	9.153(−0.3%)	12.398(3.2%)	116.38(0.9%)	1061.42(−1.3%)
PXRD	0.0001	10.791(15)	9.1798(38)	12.012(18)	115.302(34)	1075.78(53)
SCXRD	0.8(2)	10.5476(6)	9.0500(4)	11.9209(4)	115.048(4)	1030.90(9)
SCXRD	1.55(21)	10.3104(7)	8.9031(5)	11.8218(5)	114.913(6)	984.20(9)
SCXRD	2.74(29)	10.0337(12)	8.7479(7)	11.6464(7)	114.500(9)	930.21(14)
SCXRD	4.2(3)	9.807(2)	8.636(2)	11.512(1)	114.064(17)	890.3(2)
SCXRD	5.28(12)	9.663(4)	8.514(4)	11.294(4)	113.84(4)	853(4)
SCXRD	7.08(32)	9.480(6)	8.438(6)	11.039(5)	113.34(6)	810.9(1.0)
SCXRD	9.2(3)	9.340(6)	8.431(8)	10.940(8)	112.05(7)	798.5(1.0)

[a]The ambient pressure parameters were determined from a separate sample using PXRD (loading B). The remaining data are determined from SCXRD using a neon PTM in a DAC (loading A). A comparison is made with the theoretically calculated lattice parameters at 0 GPa. The percentages indicate the differences between theory and experiment at 0 GPa.
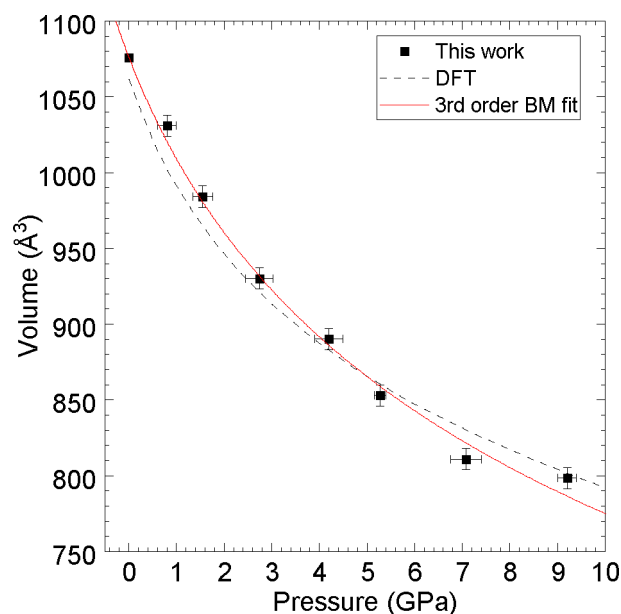
Figure 3. Unit cell volumes of TNBA as a function of pressure with corresponding error bars. The squares are the data points from single-crystal X-ray diffraction (loading A) apart from the ambient pressure point which is from a separate powder loading (loading B). The red line is a weighted third-order Birch–Murnaghan (BM) fit to all data points with V_0 fixed at 1075.8(5) Å^3, K_0 = 13.2(2.4) GPa, and K_p = 5.1(1.4). The black dashed line is the EOS determined through DFT. The DFT yields a third-order BM fit of V_0 = 1051(7) Å^3, K_0 = 14.7(1.5) GPa, and K_p = 6.0(5).

We report the third-order fit to 9.2 GPa with parameters V_0 = 1075.8(5)Å^3, K_0 = 13.2(2.4) GPa, and K_p = 5.1(1.4). The volume and lattice parameters of the ambient phase were also calculated as a function of pressure at 0 K (dashed line in Figure 3).

Absorption Measurements. During the synchrotron experiment on loading A, we observed under a microscope that compressing the TNBA sample changed it from a translucent yellow to a translucent red at ~7 GPa. To better understand the color changes occurring on compression seen in loading A, we performed white light absorption spectroscopy and Raman spectroscopy on loadings C and D.

Because previous loadings (loading F and other loadings not reported in this work) have shown evidence of helium permeation into the molecular crystal (see the Supporting Information), we loaded neon and argon PTM's into loadings C and D to verify that neon would not permeate into the crystal. Both loadings saw a phase change near the same pressure of 7 GPa, which indicates that neon permeation is not the cause of this transformation. Loadings C and D were pressurized at the same time while taking both Raman and absorption measurements at each pressure point. Figure 4 shows optical images of the sample chamber (loading C) that capture the reverse behavior upon decompression to ambient pressure.

Figure 5 shows the results of the absorption measurements of loading C in neon. Figure 5a shows an example of a typical absorption spectrum taken through the PTM (I_0 in blue) and through the sample (I multiplied by 10 in green) at a pressure of 32.4(3) GPa.

Figure 5b shows the smoothed absorption spectra (I_0/I) up to a pressure of 44.8(2) GPa. From ambient pressure to 37
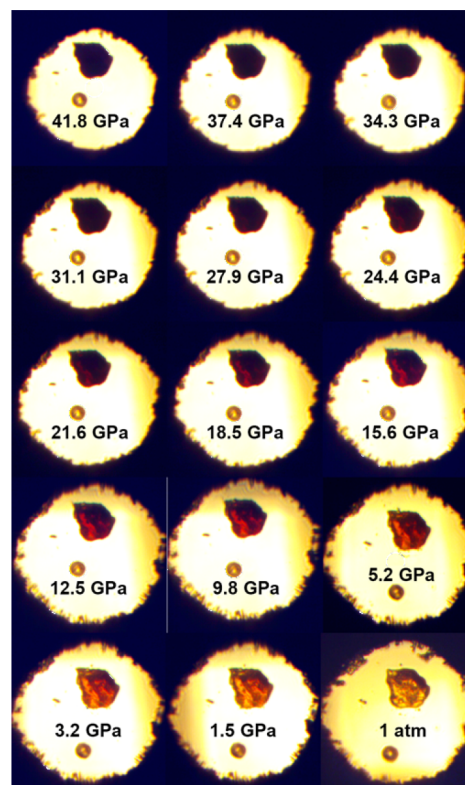

Figure 4. Optical images of the sample chamber of loading C upon decompression. The pressure transmitting medium was neon. The TNBA single crystal turns from an opaque black at 41.8 GPa to red by 21.6 GPa and then to translucent yellow at ambient pressure. The color changes are quantified by absorption measurements (see Figure 5).

GPa, we observe a consistent increase in the absorption edge (albeit a discontinuous increase at 7 GPa), where the overall shape of the absorption curve remains the same. Between 37.4(3) and 41.0(1) GPa we see a drastic change in the absorption spectra profile as the I_0/I drops from ~150 to about 90 at 600 nm. This flattening out of the intensity of the absorption remains upon decompression to ambient pressure, suggesting an irreversible change occurring at 39.2(1.8) GPa (Figure S4). This study stopped at 45 GPa due to the limits of spectral range of our optical system.

Figure 5c shows the various λ_x, where λ_x is defined as the wavelength that corresponds to I_0/I equaling x. In order for all of the data points to lie on the same curve in Figure 5c, λ_{10} has 0.23 eV added to it and λ_{40} has 0.16 subtracted from it. Between 0 and 7 GPa the absorption edge decreases in energy continuously with a slope of −74(9) meV/GPa which matches, within error, the calculated PBE-D2 band gap slope of −70(5) meV/GPa. While the slopes of the ambient structure's absorption edges with respect to pressure agree between experiment and theory, the calculated PBE-D2 band gap predicts higher overall absorption edges compared to both experimental absorption analysis methods. This is expected since PBE systemically underpredicts the band gap,[41,42] and the measured optical gap is expected to be less than the fundamental gap.[43,44] At 7 GPa the absorption edge discontinuously decreases in energy from about 2.6 to 2.4 eV, which is gigapascals above the neon crystallization pressure at room temperature (4.6 GPa), and thus we do not believe that the neon crystallization is a contributing factor to the
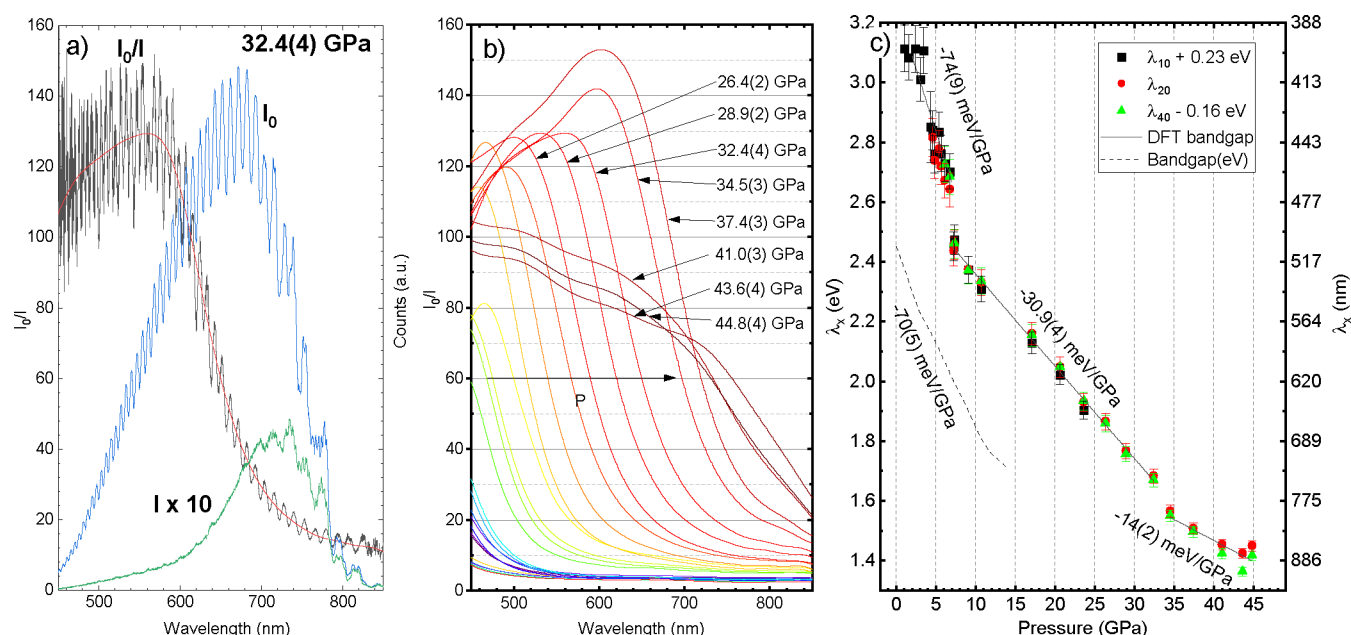
Figure 5. Absorption measurements of loading C in a neon environment. (a) An example of the raw absorption data at 32.4(3) GPa. The blue curve (I_0) is taken through the PTM, and the oscillations in the raw data are due to interference between the diamond faces. The green curve ($I \times 10$) is the absorption spectra taken through the sample and is multiplied by 10 for clarity. A 20 μm spatial filter was used for both I_0 and I, and the spatial filter was much smaller than the sample dimensions. The black curve shows the division of I_0 and I, and the red curve is the Fourier smoothing filter of I_0/I. (b) Fourier filter smoothed absorption data (I_0/I) upon compression. At the blue end of the spectrum, there are dips in the curves at the higher pressures which are due to poor signal-to-noise in that region and do not reflect the real phenomenon. There is a clear change in the absorption profiles from 37.4(1) to 41.0(1) GPa, which remains upon decompression (see Figure S4). The absorption spectra with the highest pressures are labeled by their pressures to clarify the process of the flattening of the absorption curve. (c) Pressure versus λ_x where λ_x is the wavelength where $I_0/I = x$. To have all λ_x coincide, the λ_{10} data points have 0.23 eV added to them and the λ_{40} data points have 0.16 eV subtracted from them. The dashed line is the calculated band gap at the PBE-D2 level of the ambient phase of TNBA.
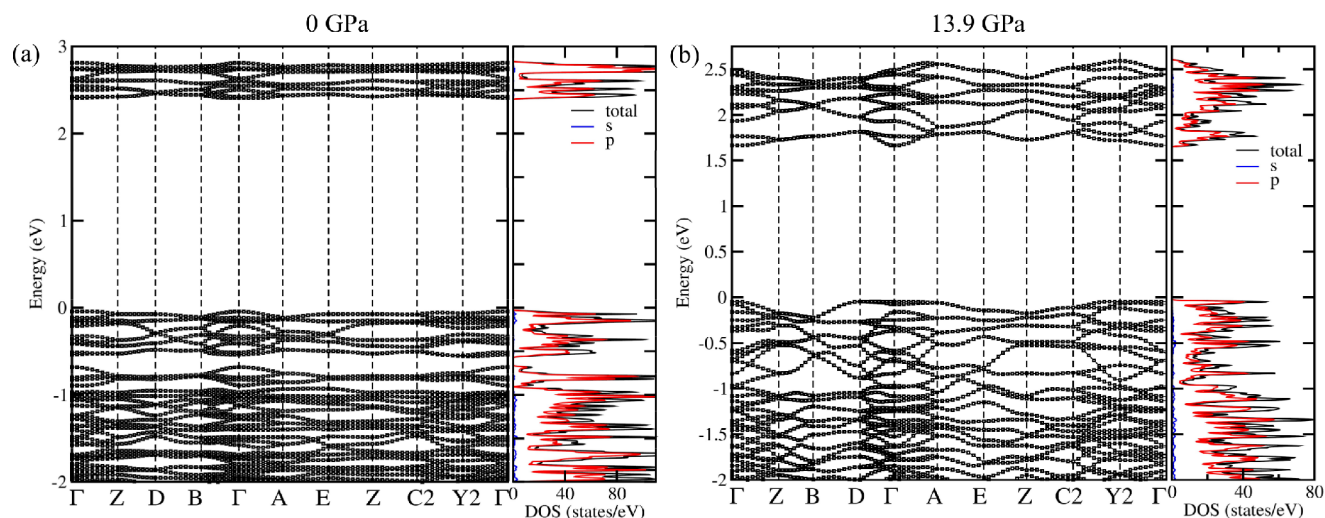
Figure 6. Electronic band structure of the ambient structure of TNBA and density of states projected on s and p orbitals at 0 and 13.9 GPa.

observed jump. Between 10 and 11 GPa there is a slight kink in the calculated pressure−volume curve as well as in the calculated lattice parameters and the calculated band gap (dashed line in Figure 5c). The kink is due to a slight structural change at high pressure where the nitro group rotates slightly to be more in the plane of the molecule and the Br−O intermolecular distance decreases by about 0.2 Å. However, the symmetry of the crystal does not change, and the change in the lattice parameters is minor. Between 7 and 33 GPa, the absorption edge decreases monotonically with a slope of −30.9(4) meV/GPa, until another jump in the absorption

edge is observed between 32.4 and 34.5 GPa. Between 34.5 and 44.8 GPa, the slope decreases further to −14(2) meV/GPa.

Decompressing loading C from 44.8(2) GPa, the absorption edge exhibits hysteresis and does not follow the same path to ambient pressure (Figures S4 and S5). The flattening of the absorption profile at 39.2(1.8) GPa, the jump in absorption at 33.5(1.1) GPa, the change in slope across this jump, and the hysteresis in the absorption edge all indicate an irreversible change (or changes) in the structure at this pressure. The profile change at 39.2(1.8) GPa is dramatic, distinct, and

5.7(1.8) GPa higher in pressure than the jump in absorption, and therefore these are likely two distinct transitions.

Electronic Band Structure. The electronic band structure calculated at the PBE+D2 level for the ambient phase of TNBA at 0 and 13.9 GPa is displayed in Figures 6a and 6b. The band structure shows that the smallest band gap is at the Γ point, it is a direct band gap, and it is dominated by p orbitals at the Fermi level and the highest unoccupied level. The bands are nearly flat, which may make indirect transitions plausible. The calculated band gap as a function of pressure is given in Figure S6, which shows the calculated band gap decreases from 2.45 to 1.71 eV from 0 to 14 GPa. Band gaps calculated at the PBE level systematically underpredict the band gap,[41] so larger band gaps are expected. To gain more insight into the electronic band structure, the projected density of states on each element was also calculated, displayed in Figure S7. At low pressure, bands near the Fermi level are dominated by oxygen p orbitals and to a lesser extent carbon and bromine p orbitals. At higher pressures, bromine has almost the same density of states at the Fermi level as oxygen. This is a rough indication that the interaction between bromine and oxygen increases at higher pressures. This also helps explain the slight structural change and kink in the lattice parameters at high pressures in the DFT calculations.

Raman Spectroscopy. In loadings C and D, Raman spectra was taken concurrently with absorption measurements at each pressure point. The Raman spectrum of TNBA at ambient pressure is shown in Figure S8. Figure 7 shows the
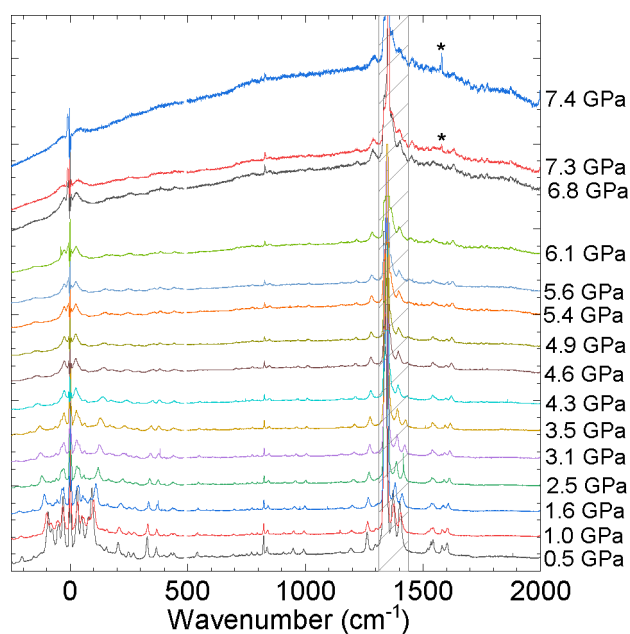
Figure 7. Raman spectra of TNBA taken in a neon environment (loading C) up to 7.4 GPa. The neon solidifies at 4.6 GPa. The gray striped box contains Raman peaks from the diamonds and ruby fluorescence. The peaks with asterisks are oxygen peaks from the atmosphere.

Raman spectra of TNBA in neon (loading C) up to 7.4(1) GPa. Starting around ~6 GPa in neon, we begin to see a broad fluorescence across the whole spectrum which increases with pressure.

Broadening of low order wavenumbers in Raman spectra with increasing pressure over the 0−7 GPa range indicates loss

of long-range lattice order, while the relative persistence of certain higher frequency wavenumbers at 823(2), 1267(2), and 1606 cm^{-1} (Figure S9) suggests that the molecules are at least partially intact. Above 7.4(1) GPa no Raman peaks can be seen (apart from the weak peaks of 823, 1267, and 1606 cm^{-1} modes). A graph of the Raman mode peak response to pressure can be found in Figure S10. This loading C was pressurized to 45 GPa and then returned back to ambient pressure. At ambient pressure the Raman peaks do not reappear, and the same fluorescent background persists (Figure S9).

Raman spectra of TNBA in argon (loading D) up to 7.8(1) GPa show the same fluorescence seen in neon (Figure S11). When we observed the fluorescence and loss of Raman in both samples at about the same pressure in different PTMs, this indicated that neon permeation into the crystal was not likely due to the difference in atomic sizes of neon and argon. At this point it was decided that to test the reversibility of this transition was more important than to take both loadings up in pressure, so the argon loading (D) was then decompressed. The fluorescent background and lack of Raman peaks of loading D remained after decompression from 7.8(1) GPa to ambient pressure which suggests an irreversible transition at 7 GPa (Figure S9). However, we still see the 824, 1267, and 1606 cm^{-1} modes indicating that the molecule is at least partially intact at 8 GPa (Figure S9).

The fluorescence and loss of Raman in loadings C and D near 7 GPa led us to ask if we were seeing a laser-induced decomposition of the sample from the Raman laser. Thus, a loading of TNBA powder in NaCl was prepared (loading E) and was taken to 8(1) GPa to test if the fluorescent background was caused by laser-induced damage from the Raman measurements. Taking Raman spectra at ambient pressure, 3.7(4) GPa, and 8(1) GPa with ≤0.2 mW of 633 nm laser light revealed the same behavior as seen in neon and argon: an increase in fluorescent background above ~6 GPa (Figure S12). Because significantly less laser power over only three pressure points yielded the same amount of fluorescence, laser-induced damage appears to not be the cause of this fluorescence. In fact, the fluorescence appears to be greater in a NaCl PTM, indicating nonhydrostatic stress to be a factor in the fluorescence.

Crystal Structure Prediction Simulations. The lack of XRD or Raman above the transition at 7−9 GPa led us to investigate the possible high-pressure phases the system was accessing. Thus, CSP calculations for molecular polymorphs were performed at 10 GPa by using the code USPEX. A summary of the search is displayed in Figure 8a−d. Figure 8a shows the relative enthalpy to the lowest enthalpy structure produced in the search as a function of the generation number, while Figures 8b−d are histograms of the energy, volume, and space group. The search produces low-enthalpy structures that consist of decomposition products such as H_2O, CO_2, and carbon chains that are energetically distinct from various TNBA molecular polymorphs.

Focusing first on the molecular polymorphs, the search produces several molecular polymorphs within a range of 5 kcal/mol lower in enthalpy than the experimental structure at 10 GPa (see Figure 8a). The lowest enthalpy polymorph has the space group $P2_12_12_1$ (space group 19) and has a herringbone-like structure displayed in Figure S13. This structure was produced in the first generation and was the lowest enthalpy polymorph for all 10 generations (see Figure
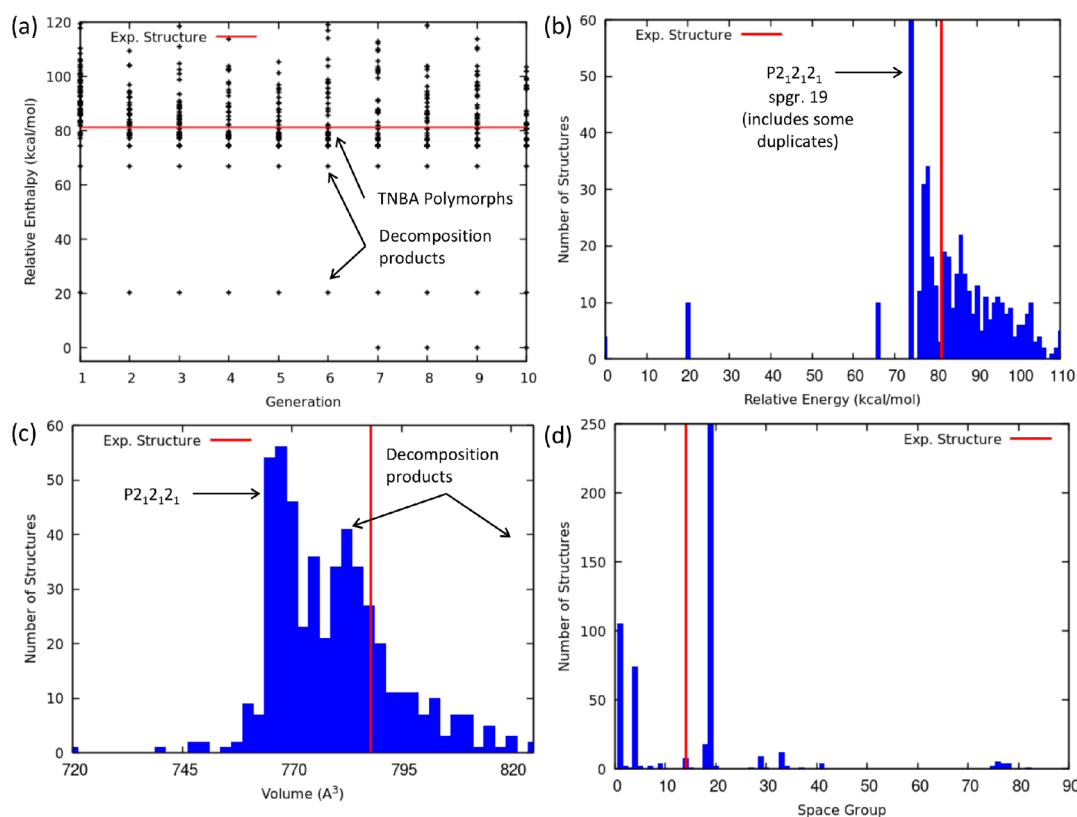
Figure 8. Summary of the results of the CSP simulations at 10 GPa for TNBA. (a) Relative enthalpy vs generation and (b−d) histograms of the enthalpy, volume, and space group of all the structures produced in the search. The energy, volume, and space group number of the ambient phase are shown at 10 GPa calculated with DFT.

8a). The histogram of the relative enthalpy shows that the number of molecular polymorphs with a lower enthalpy than the experimental structure is fairly large; however, many of these structures are duplicate structures that the code failed to distinguish from each other. Evaluation of duplicates can be improved by increasing threshold for the difference in the fingerprint function for structures to be considered unique. Nevertheless, there are a bevy of structures lower in enthalpy than the experimental structure. Examining the histograms of the volume in Figure 8c, the volume of the low-enthalpy polymorphs (including the $P2_12_12_1$ structure) are smaller than the experimental structure, which lowers the PV term in the enthalpy. The low-enthalpy polymorphs therefore represent more efficient molecular packing at 10 GPa.

While the structure search produced lower enthalpy structures than the experimental one, it is worth discussing how much of the structure space was sampled. Figure 8d shows the histogram of the space groups sampled in the search, dominated by low symmetry structures, space group 4, and space group 19. The space group of the ambient crystal structure (space group 14) was not sampled nearly as much. This is a signature of trapping, a phenomena in a genetic algorithm where the search gets trapped on a particular part of the free energy surface.

Because the experimental structure was not produced at 10 GPa, a validation search was performed at 0 GPa to test whether it could find the ambient crystal structure. Histograms of the energy, volume, and space groups from the search at 0 GPa are displayed in Figure S14a−c. The search successfully produces low-energy structures relative to the ambient structure within 1 kcal/mol; however, none of them are

lower in enthalpy than the experimentally determined structure optimized with DFT. Structures that are lower in energy consist of decomposition products. The search did not find the correct experimental structure at 0 GPa, and most structures had a volume larger than the experimental structure (see Figure S14b). This indicates the initial structure generation struggles to generate low-energy high-density structures at 0 GPa. Other methods designed to search for molecular crystals may be more effective, such as GAtor.[45] Although the experimental structure was not generated, the CSP search demonstrates there exists a thermodynamic driver for a phase transition at 10 GPa. Predicting the exact high-pressure crystal structure, the global minima on the free energy surface may still be a challenge, but the current pool of structures provides some insight into the high-pressure behavior of TNBA. Nevertheless, the search finds lower enthalpy polymorphs at high pressure but does not at 0 GPa, which is evidence in support of a pressure-induced phase transition. However, predicting the exact high-pressure crystal structure, the global minima on the free energy surface, may still be a challenge.

The CSP also produces structures that consist of decomposition products, and although the CSP does not calculate energy barriers that are important for understanding the chemistry of energetic materials, it is plausible that the relative enthalpies and molecular structures of these decomposed structures may provide insight into understanding the high-pressure chemistry. A snapshot of the structure with the lowest enthalpy in the search at 10 GPa is displayed in Figure S15. The structure consists of gas phase products H_2O, CO_2, and CHNO and other small molecules that may be representative of chemical intermediates. The search also

consists of an extended carbon, nitrogen, and oxygen chain network. The carbon chain network is also linked with CNO heterocycles. These types of structures may provide insight into the local structure of amorphous condensed carbon at high pressures. Another interesting point is that due to the extended carbon network, the volume of this structure is smaller than the volume of the ambient TNBA polymorph (see Figure 8c). This may provide insight into the reacted EOS of TNBA.

■ DISCUSSION

Among three separate techniques, XRD, Raman, and absorption, we see agreement that there is a change in the system near 7−9 GPa. This is consistent across multiple runs with different samples, and this transition is consistent with pressure-induced amorphization (PIA). Compressing TNBA in NaCl sees greater fluorescence past 7 GPa compared to in neon or argon, indicating nonhydrostatic stress is a contributing factor to the change at this pressure. Nonhydrostatic stress such as this can cause amorphization by inducing strain and defects, which can fluoresce. This deviatoric stress can induce nucleation sites for phase growth with small critical radii in local domains.[46] These induced nanoscale grains would then be X-ray and Raman amorphous. Further X-ray diffraction or X-ray absorption studies in neon at pressures higher than 10 GPa are needed to confirm the presence of nanocrystals or whether the system is amorphous.

PIA can also occur when a phase transition has a large kinetic barrier between the two phases and is exacerbated by deviatoric stress.[47] Anealing at high temperatures can sometimes allow the system to overcome large kinetic barriers and fall into its ground state phase,[47] but with energetic materials the ground state is a decomposition of the molecules. Thus, annealing at high temperatures is not feasible for these energetic molecular crystals. Crystal structure prediction calculations performed at 10 GPa show a great number polymorphs that are lower in enthalpy than the $P2_1/c$ structure. The lowest enthalpy of these solutions is a herringbone structure. It is not unreasonable to expect that the kinetic barrier between two dramatically different phases, like the ambient layered structure and a herringbone structure, is large, and thus pressure-induced amorphization and potential dissociation of the molecule is plausible at 7 GPa. To calculate this energy barrier, solid-state nudge elastic band calculations may be used, such as what was used to calculate the energy barrier for the graphite to diamond transformation.[48,49] Future experiments, such as pair distribution function and extended X-ray fine structure, can reveal whether the system is structurally amorphous and if the molecule is still intact.

If amorphization does occur at 7 GPa and because both TNBA and TATB are layered structures, the presence of bromine and the methoxy group appears to significantly lower the pressure regime of structural stability compared to TATB which is chemically stable up to at least 150 GPa.[50] While a molecule like TATB is symmetric, planar, and stacks neatly into a layered lattice, the bromine atom's interaction with neighboring nitro groups and the interaction between neighboring methyl and nitro groups in TNBA appear to frustrate the lattice structure. From the electronic band structure calculations, at higher pressures the Fermi level is mostly composed of bromine and oxygen density of states. The bromine appears to interact with the neighboring molecule's oxygen and rotate its nitro group, while in TATB all nitro

groups remain relatively coplanar. The methoxy group appears to H-bond to a neighboring oxygen in a nitro group of a neighboring molecule, although PBE+D2 underpredicts hydrogen bonding and hydrogens are invisible to XRD. Thus, the extent of this H-bonding and its effect on TNBA's structure are not clear. While TNT is in the same space group with a different setting as TNBA ($P2_1/a$), it has a herringbone structure.[51,52] 1,3,5-Trinitrobenzene is in an orthorhombic ($Pbca$) phase,[53] and just as in TNBA, the nitro groups see rotation from the plane of the molecule as they interact with neighboring molecule's hydrogens.[53] Benzene, the canonical aromatic molecule, also amorphizes near 25 GPa;[54−56] however, the structure of benzene is a herringbone structure, and a direct comparison to TNBA is ill-suited.

In addition to the transition at 7 GPa, the absorption measurements indicate transitions at 33.5(1.2) GPa and 39.2(1.8) GPa. One of these transitions could be a decomposition of the aromatic ring since the loading decompressed from 45 GPa lacks the 1267 and 1606 cm^{-1} modes while these modes remain in the loading decompressed from 8 GPa (Figure S9). The true extent of the dissociation of the TNBA molecule is unclear, and further studies are needed to verify the nature of these transitions.

There appears to be a trend of band gap closure and thus piezochromism with these aromatic molecules. Benzene, just as TNBA, will darken with pressure.[54−56] Ciabini et al. showed that this absorption edge is due to the aromatic ring buckling.[54] TATB has a closing of the band gap as well where the absorption edge closes from ∼2.5 eV at ambient pressure to ∼1.7 eV at 20 GPa.[57]

■ CONCLUSION

We have shown the ambient crystal structure of TNBA to be $P2_1/c$, a layered structure, through single-crystal X-ray diffraction at pressures up to 9.2(3) GPa. With increasing pressure, TNBA is found to undergo an irreversible transformation around 7−9 GPa as inferred from the discontinuity in the pressure−volume response from SCXRD in addition to the disappearance of Raman spectra, increase in fluorescence background, and increase in absorption edge. This transformation is consistent with amorphization; however, further X-ray diffraction or X-ray absorption studies in a neon environment at pressures higher than 10 GPa are needed to confirm if it is a truly amorphous structure or nanocrystalline. The lower enthalpy structures found to exist in TNBA at 10 GPa by CSP simulations are in support of this finding, indicating a thermodynamic driver for a phase transition. Specifically, the USPEX code has shown rich polymorphism with enthalpies within a few kcal/mol of each other at 10 GPa. Given the significantly different structure types of these polymorphs as compared to the layered ambient structure, the system could be kinetically hindered from transforming into one of these predicted polymorphs. The hypothesis of a kinetically hindered mechanism would be consistent with the pressure-induced amorphization proposed in our work. Further possible transitions are found in TNBA at higher pressures at 33.5(1.2) GPa and 39.2(1.8) GPa by using visible absorption measurements alone. The data suggest a possible dissociation of the TNBA molecule as evidenced by the disappearance of Raman modes after decompression.

Several potential directions for future studies can be proposed in light of the findings presented in this work. One direction would be to perform an extended X-ray absorption

fine structure (EXAFS) measurements on the bromine K-edge (13.47 keV), which would reveal the local coordination of the bromine atom. The atomic pair distribution function and EXAFS can reveal how intact the TNBA molecule is at higher pressures. Because fluorescence was observed with 515 nm laser light at ambient pressure, a future study could look at the fluorescence change with pressure, thereby gaining more insight into the electronic structure at high pressure. Low-temperature Raman experiments of TNBA can elucidate the anharmonic coupling between the high- and low-frequency modes,[58] which is relevant for shock conditions, where in nonequilibrium time scales the low-frequency lattice modes are populated by the shock wavefront and the high-frequency mode population affects the dissociation of the molecule.[59−62] The level of this anharmonic coupling between the lattice and molecular modes is related to the energetic material's sensitivity.[62,63] The equation of state of TNBA is valuable for modeling its detonation properties, and to track volume compressibility at pressures above 9 GPa where the sample is amorphous, a technique like optical microscopy and interferometry (OMI)[64] could be used.

ASSOCIATED CONTENT

Ⓢ Supporting Information

The Supporting Information is available free of charge at https://pubs.acs.org/doi/10.1021/acs.jpcc.1c08804.

　　Figures S1−S18 and Table S1 (PDF)

　　TNBA structure solved through SCXRD at 0.8(2) GPa (CIF)

AUTHOR INFORMATION

Corresponding Author

　　Christian M. Childs − *Physical and Life Sciences Directorate, Lawrence Livermore National Laboratory, Livermore, California 94550, United States;* ⦿ orcid.org/0000-0002-1114-0995; Email: childs6@llnl.gov

Authors

　　Brad A. Steele − *Physical and Life Sciences Directorate, Lawrence Livermore National Laboratory, Livermore, California 94550, United States;* ⦿ orcid.org/0000-0002-8703-024X

　　Paulius Grivickas − *Physical and Life Sciences Directorate, Lawrence Livermore National Laboratory, Livermore, California 94550, United States*

　　Dongzhou Zhang − *Partnership for Extreme Crystallography, University of Hawaii at Manoa, Honolulu, Hawaii 96822, United States;* ⦿ orcid.org/0000-0002-6679-892X

　　Jonathan Crowhurst − *Physical and Life Sciences Directorate, Lawrence Livermore National Laboratory, Livermore, California 94550, United States*

　　I-Feng W. Kuo − *Physical and Life Sciences Directorate, Lawrence Livermore National Laboratory, Livermore, California 94550, United States*

　　Sorin Bastea − *Physical and Life Sciences Directorate, Lawrence Livermore National Laboratory, Livermore, California 94550, United States*

　　Samantha M. Clarke − *Physical and Life Sciences Directorate, Lawrence Livermore National Laboratory, Livermore, California 94550, United States;* ⦿ orcid.org/0000-0002-6874-9929

Complete contact information is available at:

https://pubs.acs.org/10.1021/acs.jpcc.1c08804

Notes

ACKNOWLEDGMENTS

REFERENCES

(1) Fung, V.; Alexander, B.; Morris, J.; Price, D. W.; Wilmoth, R.; Systems, B. *Melt-pour Explosive Formulations Development Featuring TNBA*, 2018.

(2) Price, D. *GrIMEx (Green IM Explosive): Development of Novel IM Comp B Replacements Based on Green TNT and RDX Replacements*, 2019.

(3) Sabatini, J. J.; Oyler, K. D. Recent Advances in the Synthesis of High Explosive Materials. *Crystals* **2016**, *6*, 5.

(4) Lafourcade, P.; Denoual, C.; Maillet, J.-B. Irreversible Deformation Mechanisms for 1,3,5-Triamino-2,4,6-Trinitrobenzene Single Crystal through Molecular Dynamics Simulations. *J. Phys. Chem. C* **2018**, *122*, 14954−14964.

(5) Politzer, P.; Murray, J. S. Impact sensitivity and crystal lattice compressibility/free space. *J. Mol. Model.* **2014**, *20*, 2223.

(6) Zeman, S.; Liu, N.; Jungová, M.; Hussein, A. K.; Yan, Q.-L. Crystal lattice free volume in a study of initiation reactivity of nitramines: Impact sensitivity. *Defence Technology* **2018**, *14*, 93−98.

(7) Fabbiani, F. P. A.; Pulham, C. R. High-pressure studies of pharmaceutical compounds and energetic materials. *Chem. Soc. Rev.* **2006**, *35*, 932−942.

(8) Palmer, S. J. P.; Field, J. E.; Tabor, D. The deformation and fracture of β-HMX. *Proc. R. Soc. London. A. Mathematical and Physical Sciences* **1982**, *383*, 399−407.

(9) Ravindran, T. R.; Rajan, R.; Venkatesan, V. Review of Phase Transformations in Energetic Materials as a Function of Pressure and Temperature. *J. Phys. Chem. C* **2019**, *123*, 29067−29085.

(10) Klotz, S.; Chervin, J.-C.; Munsch, P.; Le Marchand, G. Hydrostatic limits of 11 pressure transmitting media. *J. Phys. D: Appl. Phys.* **2009**, *42*, 075413.

(11) Shen, G.; Wang, Y.; Dewaele, A.; Wu, C.; Fratanduono, D. E.; Eggert, J.; Klotz, S.; Dziubek, K. F.; Loubeyre, P.; Fat'yanov, O. V.; et al. Toward an international practical pressure scale: A proposal for an IPPS ruby gauge (IPPS-Ruby2020). *High Pressure Research* **2020**, *40*, 299−314.

(12) Dolomanov, O. V.; Bourhis, L. J.; Gildea, R. J.; Howard, J. a. K.; Puschmann, H. OLEX2: a complete structure solution, refinement and analysis program. *J. Appl. Crystallogr.* **2009**, *42*, 339−341.

(13) Sheldrick, G. M. Program for empirical absorption correction of area detector data. *Sadabs* **1996**.

(14) Prescher, C.; Prakapenka, V. B. DIOPTAS: a program for reduction of two-dimensional X-ray diffraction data and data exploration. *High Pressure Research* **2015**, *35*, 223−230.

(15) Toby, B. H.; Von Dreele, R. B. GSAS-II: the genesis of a modern open-source all purpose crystallography software package. *J. Appl. Crystallogr.* **2013**, *46*, 544−549.

(16) Momma, K.; Izumi, F. VESTA 3 for three-dimensional visualization of crystal, volumetric and morphology data. *J. Appl. Crystallogr.* **2011**, *44*, 1272−1276.

(17) Hohenberg, P.; Kohn, W. Inhomogeneous Electron Gas. *Phys. Rev.* **1964**, *136*, B864−B871.

(18) Kohn, W.; Sham, L. J. Self-Consistent Equations Including Exchange and Correlation Effects. *Phys. Rev.* **1965**, *140*, A1133−A1138.

(19) Kresse, G.; Furthmüller, J. Efficiency of ab-initio total energy calculations for metals and semiconductors using a plane-wave basis set. *Comput. Mater. Sci.* **1996**, *6*, 15−50.

(20) Blöchl, P. E. Projector augmented-wave method. *Phys. Rev. B* **1994**, *50*, 17953−17979.

(21) Kresse, G.; Joubert, D. From ultrasoft pseudopotentials to the projector augmented-wave method. *Phys. Rev. B* **1999**, *59*, 1758−1775.

(22) Perdew, J. P.; Burke, K.; Ernzerhof, M. Generalized Gradient Approximation Made Simple. *Phys. Rev. Lett.* **1996**, *77*, 3865−3868.

(23) Grimme, S. Semiempirical GGA-Type Density Functional Constructed with a Long-Range Dispersion Correction. *J. Comput. Chem.* **2006**, *27*, 1787−1799.

(24) Grimme, S.; Antony, J.; Schwabe, T.; Mück-Lichtenfeld, C. Density functional theory with dispersion corrections for supramolecular structures, aggregates, and complexes of (bio)organic molecules. *Org. Biomol. Chem.* **2007**, *5*, 741−758.

(25) Zhao, Y.; Truhlar, D. G. Benchmark Databases for Nonbonded Interactions and Their Use To Test Density Functional Theory. *J. Chem. Theory and Comput.* **2005**, *1*, 415−432.

(26) Landerville, A. C.; Conroy, M. W.; Budzevich, M. M.; Lin, Y.; White, C. T.; Oleynik, I. I. Equations of state for energetic materials from density functional theory with van der Waals, thermal, and zero-point energy corrections. *Appl. Phys. Lett.* **2010**, *97*, 251908.

(27) Landerville, A. C.; Oleynik, I. I. Vibrational and thermal properties of β-HMX and TATB from dispersion corrected density functional theory. *AIP Conf. Proc.* **2015**, *1793*, 050007.

(28) Steele, B. A.; Stavrou, E.; Prakapenka, V. B.; Kroonblawd, M. P.; Kuo, I.-F. W. High-Pressure Equation of State of 1,3,5-triamino-2,4,6-trinitrobenzene: Insights into the Monoclinic Phase Transition, Hydrogen Bonding, and Anharmonicity. *J. Phys. Chem. A* **2020**, *124*, 10580−10591.

(29) Oganov, A. R.; Glass, C. W. Crystal structure prediction using ab initio evolutionary techniques: principles and applications. *J. Chem. Phys.* **2006**, *124*, 244704.

(30) Glass, C. W.; Oganov, A. R.; Hansen, N. USPEX-evolutionary crystal structure prediction. *Comput. Phys. Commun.* **2006**, *175*, 713−720.

(31) Lyakhov, A. O.; Oganov, A. R.; Valle, M. How to predict very large and complex crystal structures. *Comput. Phys. Commun.* **2010**, *181*, 1623−1632.

(32) Zhu, Q.; Oganov, A. R.; Glass, C. W.; Stokes, H. T. Constrained evolutionary algorithm for structure prediction of molecular crystals: methodology and applications. *Acta Crystallographica Section B* **2012**, *68*, 215−226.

(33) Price, D. *GrIMEx: Development of a Novel*; Green IM Comp B Replacement, 2015; https://imemg.org/wp-content/uploads/2015/06/5B-2-PRICE-day2-imemts2015.pdf.

(34) Samuels, P.; Spangler, K.; Iwaniuk, D.; Cornell, R.; Baker, E. L.; Stiel, L. I. *Detonation performance analyses for recent energetic molecules*. St. Louis, MO, 2018; p 150033.

(35) Reinke, E. *Human Cell Line Activation Test of the Novel Energetics 2,6-pyrazinediamine 3,5-dinitro 1 − oxide (LLM-105) and 2,4,6-trinitro-3-bromoanisole (TNBA)*, 2017; p 35.

(36) Reinke, E. N.; Sikorski, A. *Microtox Toxicity Testing of the Novel Energetics, 1, 4 Dinitroglycoluril (DNGU), 3, 4 Dinitropyrazole (DNP), 1, 4, 7 trinitrohexahydro 1Himidazo [4, 5 b] pyrazine 2 (3H) on (HK 56), 2, 6 diamino 3, 5 dinitro 2, 3 dihydropyrazine1 oxide (LLM 105), and 2, 4, 6 trinitro 3 bromoanisole (TNBA)*, 2018.

(37) Ernzerhof, M.; Scuseria, G. E. Assessment of the Perdew−Burke−Ernzerhof exchange-correlation functional. *J. Chem. Phys.* **1999**, *110*, 5029−5036.

(38) Xu, X.; Goddard, W. A. The extended Perdew-Burke-Ernzerhof functional with improved accuracy for thermodynamic and electronic properties of molecular systems. *J. Chem. Phys.* **2004**, *121*, 4068−4082.

(39) Krukau, A. V.; Vydrov, O. A.; Izmaylov, A. F.; Scuseria, G. E. Influence of the exchange screening parameter on the performance of screened hybrid functionals. *J. Chem. Phys.* **2006**, *125*, 224106.

(40) Lovelace, J. J.; Murphy, C. R.; Pahl, R.; Brister, K.; Borgstahl, G. E. O. Tracking reflections through cryogenic cooling with topography. *J. Appl. Crystallogr.* **2006**, *39*, 425−432.

(41) Clark, S. J.; Robertson, J. Screened exchange density functional applied to solids. *Phys. Rev. B* **2010**, *82*, 085−208.

(42) Hasnip, P. J.; Refson, K.; Probert, M. I. J.; Yates, J. R.; Clark, S. J.; Pickard, C. J. Density functional theory in the solid state. *Philosophical Transactions of the Royal Society A: Mathematical, Physical and Engineering Sciences* **2014**, *372*, 20130270.

(43) Baerends, E. J.; Gritsenko, O. V.; van Meer, R. The Kohn−Sham gap, the fundamental gap and the optical gap: the physical meaning of occupied and virtual Kohn−Sham orbital energies. *Phys. Chem. Chem. Phys.* **2013**, *15*, 16408.

(44) Bredas, J.-L. Mind the gap! *Mater. Horiz.* **2014**, *1*, 17−19.

(45) Curtis, F.; Li, X.; Rose, T.; Vázquez-Mayagoitia, l.; Bhattacharya, S.; Ghiringhelli, L. M.; Marom, N. GAtor: A First-Principles Genetic Algorithm for Molecular Crystal Structure Prediction. *J. Chem. Theory Comput.* **2018**, *14*, 2246−2264.

(46) Yamanaka, T.; Nagai, T.; Tsuchiya, T. Mechanism of pressure-induced amorphization. *Z. Kristallogr., Cryst. Mater.* **1997**, *220*, 212.

(47) Childs, C.; Lawler, K. V.; Hector, A. L.; Petitgirard, S.; Noked, O.; Smith, J. S.; Daisenberger, D.; Bezacier, L.; Jura, M.; Pickard, C. J.; et al. Covalency is Frustrating: La2Sn2O7 and the Nature of Bonding in Pyrochlores under High Pressure−Temperature Conditions. *Inorg. Chem.* **2018**, *57*, 15051−15061.

(48) Stavrou, E.; Bagge-Hansen, M.; Hammons, J. A.; Nielsen, M. H.; Steele, B. A.; Xiao, P.; Kroonblawd, M. P.; Nelms, M. D.; Shaw, W. L.; Bassett, W.; et al. Detonation-induced transformation of graphite to hexagonal diamond. *Phys. Rev. B* **2020**, *102*, 104116.

(49) Xiao, P.; Henkelman, G. Communication: From graphite to diamond: Reaction pathways of the phase transition. *J. Chem. Phys.* **2012**, *137*, 101101.

(50) Davidson, A. J.; Dias, R. P.; Dattelbaum, D. M.; Yoo, C.-S. Stubborn" triaminotrinitrobenzene: Unusually high chemical stability of a molecular solid to 150 GPa. *J. Chem. Phys.* **2011**, *135*, 174507.

(51) Miller, G. R.; Garroway, A. N. A Review of the Crystal Structures of Common Explosives Part I: RDX, *HMX, TNT, PETN, and Tetryl*. **2001**, 33.

(52) Vrcelj, R. M.; Sherwood, J. N.; Kennedy, A. R.; Gallagher, H. G.; Gelbrich, T. Polymorphism in 2−4-6 Trinitrotoluene. *Cryst. Growth Des.* **2003**, *3*, 1027−1032.

(53) Choi, C. S.; Abel, J. E. The crystal structure of 1,3,5-trinitrobenzene by neutron diffraction. *Acta Crystallographica Section B Structural Crystallography and Crystal Chemistry* **1972**, *28*, 193−201.

(54) Ciabini, L.; Santoro, M.; Bini, R.; Schettino, V. High Pressure Photoinduced Ring Opening of Benzene. *Phys. Rev. Lett.* **2002**, *88*, 085505.

(55) Ciabini, L.; Santoro, M.; Gorelli, F. A.; Bini, R.; Schettino, V.; Raugei, S. Triggering dynamics of the high-pressure benzene amorphization. *Nat. Mater.* **2007**, *6*, 39−43.

(56) Citroni, M.; Bini, R.; Foggi, P.; Schettino, V. Role of excited electronic states in the high-pressure amorphization of benzene. *Proc. Natl. Acad. Sci. U. S. A.* **2008**, *105*, 7658−7663.

(57) Sun, X.; Wang, X.; Liang, W.; Gao, C.; Sui, Z.; Liu, M.; Dai, R.; Wang, Z.; Zheng, X.; Zhang, Z. Pressure-Induced Conformer Modifications and Electronic Structural Changes in 1,3,5-Triamino-2,4,6-trinitrobenzene (TATB) up to 20 GPa. *J. Phys. Chem. C* **2018**, *122*, 15861−15867.

(58) McGrane, S. D.; Shreve, A. P. Temperature-dependent Raman spectra of triaminotrinitrobenzene: Anharmonic mode couplings in an energetic material. *J. Chem. Phys.* **2003**, *119*, 5834−5841.

(59) Tarver, C. M. Multiple Roles of Highly Vibrationally Excited Molecules in the Reaction Zones of Detonation Waves. *J. Phys. Chem. A* **1997**, *101*, 4845−4851.

(60) Tokmakoff, A.; Fayer, M. D.; Dlott, D. D. Chemical reaction initiation and hot-spot formation in shocked energetic molecular materials. *J. Phys. Chem.* **1993**, *97*, 1901−1913.

(61) Kim, H.; Dlott, D. D. Theory of ultrahot molecular solids: Vibrational cooling and shock-induced multiphonon up pumping in crystalline naphthalene. *J. Chem. Phys.* **1990**, *93*, 1695−1709.

(62) Fried, L. E.; Ruggiero, A. J. Energy Transfer Rates in Primary, Secondary, and Insensitive Explosives. *J. Phys. Chem.* **1994**, *98*, 9786−9791.

(63) Rice, B. M.; Hare, J. J. A Quantum Mechanical Investigation of the Relation between Impact Sensitivity and the Charge Distribution in Energetic Molecules. *J. Phys. Chem. A* **2002**, *106*, 1770−1783.

(64) Stavrou, E.; Zaug, J. M.; Bastea, S.; Crowhurst, J. C. The equation of state of 5-nitro-2,4-dihydro-1,2,4,-triazol-3-one determined via in-situ optical microscopy and interferometry measurements. *J. Appl. Phys.* **2016**, *119*, 135904.

⊞ Recommended by ACS